Journal of Colloid and Interface Science 437 (2015) 205–210

Contents lists available at ScienceDirect

Journal of Colloid and Interface Science

www.elsevier.com/locate/jcis

Magnetic orientation of nontronite clay in aqueous dispersions and its effect on water diffusion

Christoffer Abrahamsson [a,b,*], Lars Nordstierna [a], Matias Nordin [c], Sergey V. Dvinskikh [d,e], Magnus Nydén [f]

[a] Applied Surface Chemistry, Department of Chemical and Biological Engineering, Chalmers University of Technology, Kemivägen 10, 412 96 Gothenburg, Sweden
[b] SuMo Biomaterials, VINN Excellence Centre, Chalmers University of Technology, 412 96 Gothenburg, Sweden
[c] German Cancer Research Center, Medical Physics in Radiology, Im Neuenheimer Feld 280, 69120 Heidelberg, Germany
[d] Department of Chemistry, KTH Royal Institute of Technology, Teknikringen 30, 100 44 Stockholm, Sweden
[e] Laboratory of Biomolecular NMR, St. Petersburg State University, St. Petersburg 199034, Russia
[f] Ian Wark Research Institute, University of South Australia, Mawson Lakes Campus, Mawson Lakes, SA 5095, Australia

ARTICLE INFO

Article history:
Received 13 June 2014
Accepted 15 September 2014
Available online 28 September 2014

Keywords:
Nontronite clay
Magnetic alignment
Exfoliated clay
Anisotropic microstructure
Diffusion
Permeability
Bound water
NMR 1D imaging
Diffusion NMR

ABSTRACT

The diffusion rate of water in dilute clay dispersions depends on particle concentration, size, shape, aggregation and water-particle interactions. As nontronite clay particles magnetically align parallel to the magnetic field, directional self-diffusion anisotropy can be created within such dispersion. Here we study water diffusion in exfoliated nontronite clay dispersions by diffusion NMR and time-dependant 1H-NMR-imaging profiles. The dispersion clay concentration was varied between 0.3 and 0.7 vol%. After magnetic alignment of the clay particles in these dispersions a maximum difference of 20% was measured between the parallel and perpendicular self-diffusion coefficients in the dispersion with 0.7 vol% clay. A method was developed to measure water diffusion within the dispersion in the absence of a magnetic field (random clay orientation) as this is not possible with standard diffusion NMR. However, no significant difference in self-diffusion coefficient between random and aligned dispersions could be observed.

1. Introduction

Clay dispersions are widely used in for example oil well drilling [1], food packaging [2] and sealing barriers for waste dumps [3] or nuclear waste containment [4]. Colloidal clay dispersions, hydrogels and composites have during the last two decades emerged as possible alternatives to fossil fuel derived polymer solutions and gels [5–7].

Nontronite clay is a naturally occurring aluminosilicate mineral consisting of 0.7 nm thick and typically 25–1000 nm wide plates consisting of two tetrahedral layers of silica sandwiching an octahedral layer that hosts different ions (Al^{3+}, Mg^{2+} and Fe^{3+}). Being rich in Fe(III) ions, nontronite align in both electric [8] and magnetic fields [9–12]. Clay dispersions typically contain aggregates of face-to-face stacked clay plates. However, under certain conditions these can be separated (exfoliated), forming dispersions of individual clay plates. Michot and co-workers found isotropic, biphasic and nematic phases, and ultimately birefringent gels when increasing the clay concentration in dilute exfoliated nontronite clay dispersions [10].

Due to their extreme surface-to-volume ratios clay plates are very effective for obstructing/slowing down the diffusion of solutes and solvents, an effect that can be tuned by the plate orientation [12–17]. Additional factors that affect the particle diffusion obstruction are shape, volume fraction, size distribution, and aspect ratio [5,18–20]. The aspect ratio is defined as the average diameter divided by the thickness. Furthermore, solute and solvent diffusion is affected by interactions with the clay surfaces [13,21,22].

In a previous study we studied clay alignment and water diffusion in gels made from clay and colloidal silica, taking into account obstruction but also water surface interactions using the following equation [13],

$$\frac{D}{D_0} = \frac{1}{1+\frac{\alpha}{3}\left(S+\frac{1}{2}\right)\phi_{clay}} \frac{1-\phi_{clay+bound}}{1-\phi_{clay}} \quad (1)$$

where ϕ_{clay} is the clay volume fraction and $\phi_{clay+bound}$ the combined volume fraction of the clay and the surface bound water, and α the

* Corresponding author at: Applied Surface Chemistry, Department of Chemical and Biological Engineering, Chalmers University of Technology, Kemivägen 10, 412 96 Gothenburg, Sweden. Fax: +46 31 160 062.
E-mail address: abrahamc@chalmers.se (C. Abrahamsson).

http://dx.doi.org/10.1016/j.jcis.2014.09.031
0021-9797/

aspect ratio. The order parameter S is $-1/2$, 0 and 1, for parallel, random and perpendicular plate orientation, respectively, relative the direction of the diffusive flux.

Detailed studies of water diffusion in clay systems with isotropic/anisotropic microstructure increase the overall understanding of the microstructure–diffusion relationship, solvent/solute surface interactions and aggregation in soft porous materials. This report investigates clay alignment and water diffusion in nontronite clay dispersions and the findings are discussed in terms of clay orientation, particle–particle aggregation and water surface interactions.

2. Experimental

2.1. Preparation and characterization of clay dispersion

A detailed description for the preparation and characterization of nontronite clay dispersions has been reported by us earlier [13]. In short, nontronite clay was obtained from Excalibur Mineral Corp., Peekskill, NY, from the source of Allentown, PA, having the following [23] general formula $[Na_{0.3}Fe_2^{3+}(Si, Al)_4O_{10}(OH)_2{\cdot}nH_2O]$ and an estimated unit cell density of 3 g/cm^3. Clay identity and purity were validated with IR-spectroscopy and X-ray diffraction. The clay was first ground, secondly dispersed in 1M NaCl solution, followed by ultracentrifugation at 35,000*g*, where the second step was repeated three times followed by redispersion in deionized water. Sample dialysis was performed against deionized water until no change in conductivity was observed, after which the dispersion was placed in Imhoff cones for 72 h to sediment mineral impurities. Dispersions were size fractioned by centrifugation at incrementally higher *g*-forces, using 6400 and 17,000*g*. The clay pellet obtained after the last centrifugation was used in this study. A drop of 0.01 vol% clay dispersion was air-dried on a formvar and carbon-coated copper grid (Ted Pella Inc, Redding, CA, USA) prior to transmission electron microscopy (JEOL 1200EX II microscope, JEOL, Tokyo, Japan) at 120 kV to image and estimate the nontronite size distribution. Clay particles had a plate lath shape and the width and length dimensions had a log-normal distribution. Defining the clay plates' diameter as (length + width)/2, a regression analysis from the size distributions obtained from TEM gave a mean diameter of 228 with a standard deviation of 103 nm. Previous studies of exfoliated nontronite clay give an estimated plate thickness of 0.7 nm [9,10] that together with the obtained mean diameter results in a mean clay plate aspect ratio of 326 and standard deviation of 147 nm. Clay gelation was assessed by an inverted tube test, where a 0.5 ml clay dispersion in a 5 mm NMR tube was defined as a dispersion if it flowed when inverting the tube, and a gel if not. Square glass microcapillaries with 1 mm sides (CM Scientific Ltd, Silsden, UK) were filled with 0.3 vol% clay solution and imaged for birefringence with a digital camera (Olympus, FE-360) between crossed polarizers in a 0.72 Tesla magnetic field. The magnetic field was generated in the gap between two rare-earth neodymium permanent magnets and the magnetic field strength was measured with a Hall-sensor.

2.2. NMR self-diffusion measurements

The self-diffusion of H_2O water, from here on referred to as H_2O, was measured in clay dispersions in the absence of the rest of the membrane system (See further bellow) with a Bruker Avance III 500 spectrometer (Bruker, Fällanden, Switzerland) equipped with Mic5 micro-imaging probe and a 5 mm 1H RF coil. Clay dispersions with 0.3, 0.5, and 0.7 vol% clay were prepared in 5 mm NMR tubes and the self-diffusion coefficient was measured both in the direction parallel and perpendicular to the external magnetic field, denoted $D_{||}$ and $D_{\perp}$, respectively. Using the conventional PGSTE-LED sequence [24], all diffusion experiments were performed at 23 °C with 50 ms diffusion time, 0.5 ms gradient pulse length, and 160 G/cm maximum gradient strength. Trapezoidal gradient pulses with ramping time of 0.1 ms and stabilization time of 0.1 ms was used. The LED time was set to 10 ms and the gradient strength was calibrated by diffusion experiments on pure H_2O at 23 °C and 25 °C. The estimated self-diffusion coefficients measurement error was $\pm 1 \times 10^{-11}$ m^2/s.

2.3. NMR 1D imaging

To understand the effect of clay orientation on water diffusion in nontronite dispersions we intended to study diffusion in the parallel, perpendicular and random states as earlier described in connection to Eq. (1). However, the very strong magnetic field in the NMR spectrometer (14.1 Tesla) does not allow the measurement of the self-diffusion coefficient in the random state, D_{random}, in dilute nontronite dispersions due to the very fast alignment process once the sample is placed inside the magnet. Instead an indirect method was used to measure the diffusion coefficients from the mass transport across a clay dispersion membrane in the presence (D_{am}) and absence (D_{nam}) of a magnetic field. The diffusion process across the membranes is referred to as membrane diffusion, which is in contrast to the self-diffusion as measured by the NMR self-diffusion technique in the clay dispersions.

Compared to the self-diffusion coefficient, the membrane diffusion coefficient was affected by the presence of two cellulose films that kept the clay dispersion inside the membrane. However, as Eq. (2) shows this effect cancels out by normalization in the calculation of D_{random} as,

$$\frac{D_{||}}{D_{\text{random}}} = \frac{D_{\text{am}}}{D_{\text{nam}}} \tag{2}$$

The custom-made membrane system in Fig. 1 was made out of polyether ether ketone (PEEK) plastic. Two regenerated cellulose membranes (Spectrum Labs, Spectra/Por, MWCO 12-14000) were cut from a larger membrane disk and glued with polyacrylate glue to the separating spacer ring, forming a 1.2 mm thick membrane while the hole in the center of the ring had a diameter of 3 mm. The space confined by the spacer ring and the cellulose membranes were filled with 0.7 vol% clay dispersion from a syringe with a needle. The system was assembled according to Fig. 1, after which the upper chamber (donor chamber) and lower (receiver chamber) were rinsed with deuterium oxide water (99.8 atomic% deuterium, from here on referred to as D_2O) and equilibrated with D_2O for 30 min to exchange and remove the H_2O present in the clay dispersion within the membrane. The receiver chamber was then filled with pure D_2O and sealed from the bottom with a polydimethylsiloxane (PDMS) plug. The donor chamber was rinsed and filled with a 1:1 volume mixture of D_2O and H_2O (MilliQ water, Millipore, 18 MΩ cm) and Parafilm M® was used to seal the chamber. A 10 mm NMR glass tube was attached to the top of the membrane system, where the rubber ring ensured a mechanically secure fit between the glass tube and membrane system. Both the upper and lower chambers shown in Fig. 1 are cylindrical and 3 mm in diameter and 8 mm in length.

For the imaging measurement the membrane system was placed in a Bruker Avance 600 spectrometer (Bruker, Fällanden, Switzerland) equipped with Diff30 diffusion probe and a 10 mm RF insert coil. Inside the NMR magnet the membrane experienced a temperature of 23 °C and a magnetic field of 14.1 Tesla perpendicular to the plane of the membrane. Allowing for diffusion of H_2O/D_2O over the membrane, instant 1D-proton intensity profiles were recorded at different time points over 6 h and 12 min using a standard 90/180° spin-echo 1D-image profile pulse sequence with 12 G/cm gradient pulses. Following magnitude calculation of the

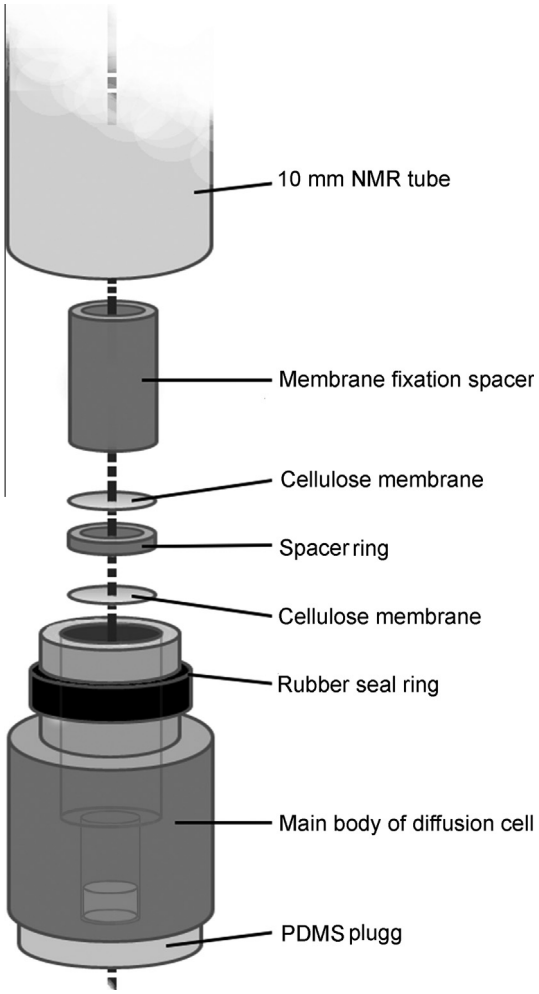

Fig. 1. Exploded schematic view of NMR membrane system.

spectrum, the final amplitude of the profile was given as function of distance z along the length of the membrane system [22,25].

For measurement of D_{nam} the membrane system was placed away from the NMR magnet for 6 h and 12 min at 23 °C, before it was placed in the NMR spectrometer. The profile recording procedure was identical to that above (D_{am}) and started immediately after the membrane system was placed in the spectrometer. Note that NMR magnetic field aligned the clays directly in the presence of the magnetic field and thus the clays were aligned when the profile was recorded for the non-aligned clay membrane. However, the profile was recorded within minutes after inserting the non-aligned membrane system into the spectrometer and therefore the increase in H_2O flux because of clay alignment contributed negligible to the concentration of H_2O in the chambers.

2.4. NMR 1D imaging data processing

Due to magnetic susceptibility inhomogeneity within the membrane system and the iron containing clay dispersion a z-dependent correlation factor was applied to the intensity profiles to obtain a normalized concentration profile with true water ^1H magnetization intensity. The correction factor was obtained from standard curves measured with known H_2O/D_2O compositions at both sides of the membrane. In total 11 profiles were recorded at H_2O concentrations between 0 and 50 vol%. A linear dependence between the H_2O concentration and intensity and the derivative ($d_{concentration}/d_{intensity}$) was used as the z-correction factor to obtain the H_2O concentration profiles from the intensity profiles. Note that water will exist in the form of HDO, but for the sake of the discussion we will refer to the diffusion in terms of H_2O and D_2O.

2.5. Diffusion modelling in membrane system

The water transport through the membrane system was modelled with a three compartment model comprising two water compartments with freely diffusing water separated by a membrane compartment modelled with a lower diffusion coefficient, D_m. The free water was modelled using a self-diffusion coefficient of 1.86×10^{-9} m^2/s which roughly corresponds to a 0.37% mixture of H_2O and D_2O at a temperature of 23 °C [26]. This value approximates the slight drift of the diffusion coefficient due to change in concentration of H_2O and D_2O during the mixing of the two compartments [27]. To find the membrane diffusion coefficient of water the coupled partial differential equations for the three compartment system was solved numerically by varying the diffusion coefficient, D_m. An optimum fit to the experimental data was obtained for the aligned and random membrane respectively by minimizing the residual in a least square sense using D_m as a parameter. The signal was distorted near to the clay containing membrane as well as the outer edges of the water compartments, due to internal gradients. The distorted regions were excluded from the fitting and the residual was taken in the remaining regions of the donor and receiver chambers as illustrated in Supporting Fig. S1.

Diffusion Eq. (3) was used to model the water diffusion through the membrane system [28],

$$\frac{\partial}{\partial t}c(z,t) = D(z)\frac{\partial^2}{\partial z^2}c(z,t) \tag{3A}$$

where c denotes the concentration and $D(z)$ the diffusion coefficient. The diffusion coefficient varies according to,

$$D(z) = \begin{cases} D_0 & |z| > l \\ D_m & |z| \leqslant l \end{cases} \tag{3B}$$

where D_0 denotes the free water diffusion coefficient and D_m the effective diffusion coefficient in the membrane. As described before D_m is denoted as D_{am} in the presence and D_{nam} in the absence of a magnetic field. l denotes half the width of the membrane. By assuming that the concentration is continuous over the membrane and assuming that no water leaves the system,

$$\frac{\partial}{\partial z}c(z=-z_0,t) = -\frac{\partial}{\partial z}c(z=z_0,t) = 0 \tag{3C}$$

(where $\pm Z_0$ denotes the exterior boundaries) together with the initial condition,

$$c(-z_0 \leqslant z \leqslant -l) = c_0 \tag{3D}$$

a unique solution can be found.

3. Results and discussion

3.1. Clay dispersion phase behavior

Viewed between crossed polarizers the nontronite clay dispersion with 0.3 vol% clay concentration showed optical flow birefringence after shaking that indicates the presence of regions with local collective alignment of clay particles. The birefringence disappeared within minutes when the sample was at rest, indicating that oriented regions relaxed back to random clay orientation. During a 5 day observation time the 0.5 vol% clay sample was a birefringent viscous dispersion while the 0.7 vol% clay sample was a birefringent gel (data not shown). Nontronite clay dispersions have

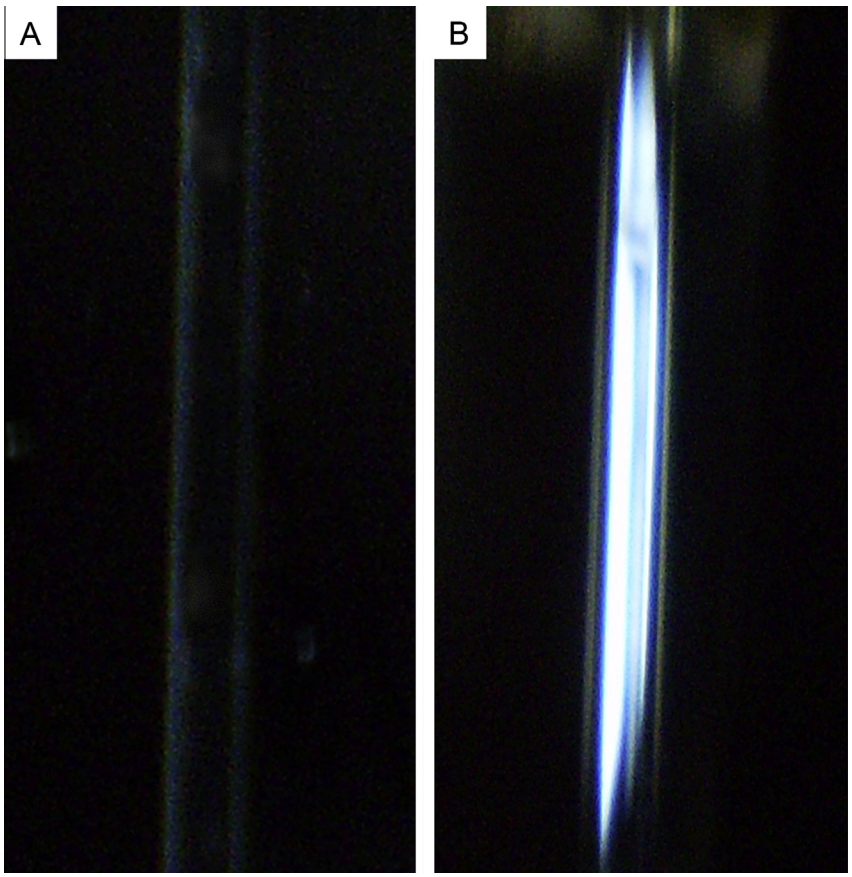

Fig. 2. A 1 mm square glass capillary filled with a 0.3 vol% nontronite clay dispersion viewed between crossed polarizers. (A) Capillary filled with the clay dispersion before exposure to magnetic field (B) capillary after 2 min of exposure to a 0.72 Tesla magnetic field. The magnetic field direction is perpendicular to the length of the capillary.

been shown to phase separate under certain circumstances if left to stand for weeks or months, resulting in an isotropic/nematic phase coexistence [10]. In this study no phase separation was observed for at least a week after shaking the dispersions and thus phase separation during the NMR measurements could be ruled out. Phase separation during an NMR experiment would have resulted in uneven clay distribution that could have affected the accuracy of our diffusion measurements.

3.2. Magnetic alignment of clay dispersions

Dilute nontronite clay dispersions are known to align in less than a minute in strong magnetic fields generated by NMR magnets [10,13]. To investigate clay alignment at a more moderate field strengths, permanent magnets were used to generate a 0.72 Tesla field. This field caused a birefringence intensity increase up to 2 min for a 0.3 vol% clay dispersion. The birefringence intensity before and after magnetic exposure is shown in Fig. 2. Within seconds after removing the sample from the magnetic field the birefringence was lost. However, one hour of 0.72 Tesla magnetic field exposure did not increase the birefringence for the 0.5 vol% clay sample. This is probably because the structural relaxation time rises strongly when the clay concentration increases [12]. Such observations fits well with the phase behavior observations discussed above, where the 0.3 vol% sample was an optically isotropic dispersion and the 0.5 vol% sample was a birefringent viscous dispersion. Fig. 3 proves that clay alignment is achievable at a higher clay concentration than 0.3 vol% in 14.1 Tesla magnetic fields. The figure shows that distinctly different diffusion coefficients, parallel ($D_{||}$) and perpendicular ($D_{\perp}$), were obtained and that $D_{||}$ always was larger than $D_{\perp}$.

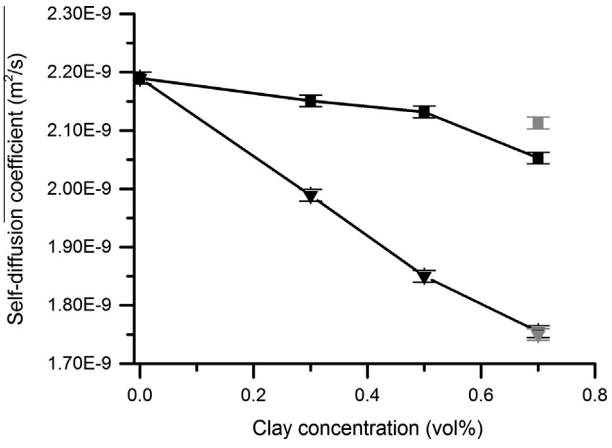

Fig. 3. Self-diffusion coefficient of H_2O measured in clay dispersions with diffusion NMR in the direction parallel (squares) or perpendicular (triangles) with the magnetic field. Samples were placed for 0.5 h in the spectrometer before measurement (black symbols), except for the 0.7 vol% clay sample where an additional time point at 36 h is presented (gray symbols). The error bars depict the estimated experimental error.

Fig. 4 shows that the diffusion coefficient difference ($D_{||}$ vs. $D_{\perp}$) was growing over time for the 0.7 vol% sample. $D_{||}$ was 17% larger than $D_{\perp}$ 0.5 h after magnetic field exposure and 20% larger after 36 h. This is also the largest diffusion coefficient difference measured in the study. The slow alignment in the 0.7 vol% sample is in contrast with both the 0.3 and 0.5 vol% sample, respectively, that displayed a stable diffusion coefficient difference already after 30 min of strong magnetic field exposure. The 0.7 vol% sample is

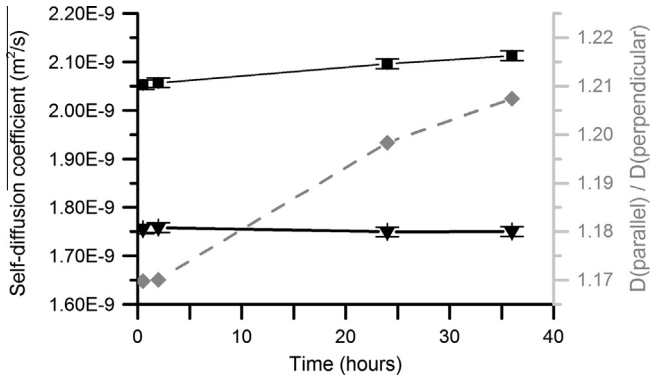

Fig. 4. Self-diffusion coefficient of H_2O as a function of time measured with diffusion NMR in a 0.7 vol% clay dispersion in the direction parallel (black squares) or perpendicular (black triangles) to the magnetic field. The gray diamonds show the ratio between the diffusion coefficients parallel and perpendicular to the magnetic field. The error bars depict the estimated experimental error.

a birefringent gel while the 0.5 vol% sample is a viscous dispersion that is considerably less viscous than the 0.7 vol% clay gel. The difference in viscosity is the most probable reason why the 0.5 vol% sample aligns significantly faster. The difference in $D_{||}$ vs. $D_{\perp}$ confirms that the clays were oriented parallel to the magnetic field. This was further confirmed by holding crossed polarizer slit gratings at different angles relative the aligned sample shown in Fig. 2. Light extinction conditions were found parallel with the magnetic field, supporting that the clays indeed are oriented in the direction of the magnetic field in correspondence with previous studies [12,13,29].

The thickness of the bound water layer can be estimated from the decrease in $D_{||}$ with increasing clay concentration. Using Eq. (1) with $S = -1/2$, the found $\phi_{clay+bound}$ value corresponds to a fitted bound water layer thickness of 1.8 ± 0.29 nm which is similar to what have previously been reported for clay dispersions in the literature [30–32]. We have in the past reported a bound water layer thickness of 1.4 nm in 0.5 vol% clay nontronite gels with 1 M ammonium bicarbonate [13]. In these gels the high salt concentration screened the nontronite clay surface charges and thereby also the thickness of the bound water layer [33]. It should be stressed that perfect alignment of clays is never achieved in practice [11], even if it is a fair approximation in dilute nontronite samples exposed to very high magnetic fields and allowing enough time for alignment.

The amount of bound and free water in the samples was identical when measuring both $D_{||}$ and $D_{\perp}$. Furthermore, the ratio of $D_{||}$ and $D_{\perp}$ depends only on the degree of clay alignment and aggregation. To find the effective aspect ratio, α, and the degree of clay aggregation we have previously [13] employed the ratio of Eq. (1) for different clay orientations. With regard to parallel and perpendicular orientation the ratio $D_{||}/D_{\perp}$ yields,

$$\frac{D_{||}}{D_{\perp}} = 1 + \frac{\alpha}{3}\phi_{clay} \tag{4}$$

The data from Fig. 4 were used to find the ratio $D_{||}/D_{\perp}$ versus clay volume fraction. The linear pattern strictly follows Eq. (4) and a linear regression analysis resulted in an aspect ratio $\alpha = 87.3 \pm 3.8$. A model was then used to estimate the degree of clay aggregation in which the following assumptions were made: (1) complete clay alignment and face-to-face packing of the aggregated clay plates and (2) a 1.56 nm thick layer of non-exchangeable water between the plates. (3) Clay plates have a mean diameter of 228 nm and a 0.7 nm thickness. This results in 1.84 plates in the average clay aggregate, which is close to the number previously found in nontronite dispersions and gels [12,13,34].

3.3. Imaging concentration profiles

1D–1H-profiles were measured over the custom made membrane system illustrated in Fig. 1. As described earlier the purpose of these measurements was to indirectly measure D_{random} that was not possible to measure by a standard diffusion NMR measurement as the nontronite clay plates align quickly in magnetic fields. Using the membrane system the diffusion over a membrane containing clay dispersion could be measured by monitoring the amount of H_2O that passed from the donor chamber, through the clay dispersion-filled membrane and into the receiver chamber that initially contained only D_2O.

When the H_2O–D_2O mixture was added to the donor chamber the H_2O molecules immediately started to diffuse over the membrane. The imaging concentration profiles in Figs. 5 and 6 visualize the H_2O concentration along the z-axis which is the length axis of membrane system. Fig. 5 shows the H_2O concentration profiles measured at different time points during one experimental run. Fig. 6 on the other hand shows the H_2O concentration profiles after 6 h and 12 min for several experimental runs both in the presence and absence of a magnetic field. Profile disturbances are seen in and around the membrane region as well as in the top and bottom of the chambers. Profile disturbances outside the membrane region were successfully removed from the concentration profiles by normalization against standard curves at known proton concentrations.

Supporting Fig. S1 shows the simulation and fitting to the measured H_2O concentration profiles that were made to determine the membrane diffusion coefficients for the magnetically aligned membrane. Averaging over three separate experiments the diffusion coefficient D_{am} was found to be 4.89×10^{-10} m^2/s with 11% variation between the experiments. Hence the measured value of D_{am} was about four times smaller than $D_{||}$ even though both are measured at the same clay concentration. We attribute the difference to the additional obstruction to diffusion provided by the cellulose membranes that keep the clay dispersion inside the membrane, see Fig. 1. This additional obstruction is assumed to be identical in the presence and absence of a magnetic field.

The determination of D_{random} by measuring the ratio D_{am}/D_{nam} was not possible as there was no significant difference between the H_2O concentration profiles in the presence and absence of a magnetic field, see Fig. 6. It is possible that the membrane system method is not sensitive enough to detect the difference between D_{am} and D_{nam} even for the highest clay concentration used in this study, which is expected to have the largest diffusion coefficient difference. The relative difference between D_{am} and D_{nam} should be smaller than the 20% difference measured between $D_{||}$ and $D_{\perp}$.

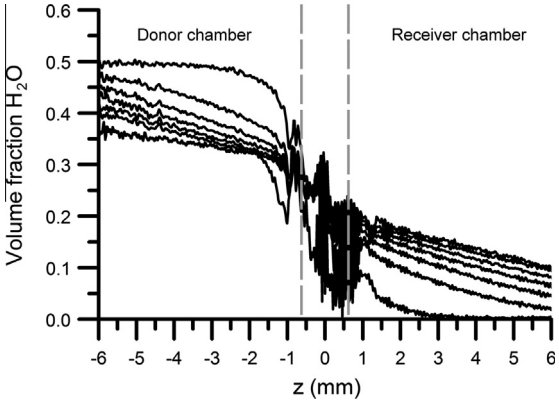

Fig. 5. Imaging H_2O concentration profiles recorded at 60 min intervals up to 372 min in total at different time points for the membrane aligned in a magnetic field. The first profile is recorded 12 min after the addition of H_2O. The dashed gray lines delimit the boundaries of the membrane.

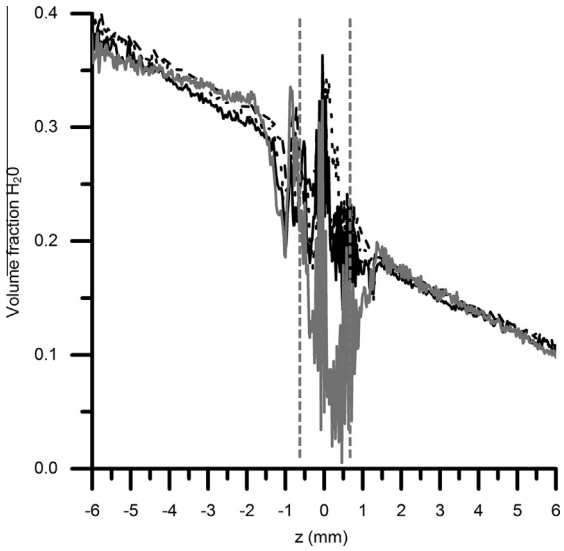

Fig. 6. Imaging H_2O concentration profiles 6 h and 12 min after initiation of experiment, comparing a membrane that has not been exposed to a magnetic field (solid grey curve) with three profiles from repeated measurements on the magnetically aligned membrane (solid, dashed and dotted black curve). The dashed gray lines delimit the boundaries of the membrane.

Thus the difference between D_{am} and D_{nam} is close to the detection limit of the membrane system method as there was an 11% variation in between the experimental runs when repeating the same experiment.

Another reason could be that the clay particle orientation is influenced by the surfaces inside the membrane. Such effects have been observed in nematic clay dispersions close to glass walls by De Azevedo and colleagues [14,15]. Such effects could drive regions of the clay dispersions close the cellulose membrane surfaces to be oriented perpendicular to the magnetic field, which would reduce the difference between D_{am} and D_{nam}. Further studies of how bulk material surfaces induce clay alignment in the adjacent nontronite dispersion while exposed to magnetic fields seem warranted.

4. Conclusions

In this study we have investigated the effect of clay particle alignment, aggregation and surface interactions on the diffusion of water in dilute nontronite clay dispersions. Our study shows that a relatively large diffusion anisotropy is obtained by aligning the clay particles in a magnetic field. These measurements made it possible to estimate the thicknesses of the bound water layer and the degree of clay aggregation. The time it takes for particles to align once placed inside the magnetic field depends strongly on the clay concentration, which puts a limit to how large directional self-diffusion anisotropy that can be practically achieved at a certain clay concentration. In previous work self-diffusion of water was studied in aligned and non-aligned composite clay gels [13]. The study presented here complements this work by successfully measuring the self-diffusion coefficients in dispersions with clays aligned both parallel and perpendicular to the magnetic field. Interestingly, the thickness of the bound water layer and the degree of clay aggregation in the dispersions presented here were similar to what was earlier found in composite gels [13].

The comparison of solvent diffusion characteristics in dispersions and gels with aligned and randomly oriented clay particles provides valuable information about colloidal systems, and soft matter overall. It helps us to understand the effect of obstruction, surface interactions and aggregation in such systems. This is important when designing materials such as fuel cells, catalysts and batteries.

Acknowledgments

We gratefully acknowledge VINNOVA for their financial support of this study through the VINN Excellence Centre SuMo Biomaterials. The Swedish NMR Center was acknowledged for spectrometer time and Diana Bernin and Jan-Erik Löfroth for their valuable input during discussions. We also thank Kurt Löfgren for his help with constructing the NMR membrane system.

Appendix A. Supplementary material

Supplementary data associated with this article can be found, in the online version, at http://dx.doi.org/10.1016/j.jcis.2014.09.031.

References

[1] G. Maitland, Curr. Opin. Colloid Interface Sci. 5 (2000) 301–311.
[2] H.H. Murray, Appl. Clay Sci. 17 (2000) 207–221.
[3] C.H. Benson, H. Zhai, X. Wang, J. Geotech. Eng. 120 (1994) 366–387.
[4] F. Madsen, Clay Miner. 33 (1998) 109–129.
[5] W.R. Falla, M. Mulski, E. Cussler, J. Membr. Sci. 119 (1996) 129–138.
[6] P. Schexnailder, G. Schmidt, Colloid Polym. Sci. 287 (2009) 1–11.
[7] Q. Wang, J.L. Mynar, M. Yoshida, E. Lee, M. Lee, K. Okuro, K. Kinbara, T. Aida, Nature 463 (2010) 339–343.
[8] R. Uhlhorn, O. Gaddy, Proc. IEEE 56 (1968) 1140–1141.
[9] L.J. Michot, I. Bihannic, S. Maddi, C. Baravian, P. Levitz, P. Davidson, Langmuir 24 (2008) 3127–3139.
[10] L.J. Michot, I. Bihannic, S. Maddi, S.S. Funari, C. Baravian, P. Levitz, P. Davidson, Proc. Natl. Acad. Sci. 103 (2006) 16101–16104.
[11] E. Paineau, K. Antonova, C. Baravian, I. Bihannic, P. Davidson, I. Dozov, M. Impéror-Clerc, P. Levitz, A. Madsen, F. Meneau, J. Phys. Chem. B 113 (2009) 15858–15869.
[12] P. Porion, A.M. Faugère, L.J. Michot, E. Paineau, A. Delville, J. Phys. Chem. C 115 (2011) 14253–14263.
[13] C. Abrahamsson, L. Nordstierna, J. Bergenholtz, A. Altskär, M. Nydén, Soft Matter 10 (2014) 4403–4412.
[14] E. De Azevedo, M. Engelsberg, J. Fossum, R. De Souza, Langmuir 23 (2007) 5100–5105.
[15] E.N. de Azevedo, M. Engelsberg, Langmuir 25 (2008) 1175–1180.
[16] P. Porion, S. Rodts, M. Al-Mukhtar, A.-M. Faugère, A. Delville, Phys. Rev. Lett. 87 (2001) 208302.
[17] T. Takahashi, T. Ohkubo, Y. Ikeda, J. Colloid Interface Sci. 299 (2006) 198–203.
[18] J.P. DeRocher, B.T. Gettelfinger, J. Wang, E.E. Nuxoll, E. Cussler, J. Membr. Sci. 254 (2005) 21–30.
[19] D.M. Eitzman, R. Melkote, E. Cussler, AIChE J. 42 (1996) 2–9.
[20] N.K. Lape, E.E. Nuxoll, E. Cussler, J. Membr. Sci. 236 (2004) 29–37.
[21] E. Cheever, F.D. Blum, K.R. Foster, R.A. Mackay, J. Colloid Interface Sci. 104 (1985) 121–129.
[22] F.P. Duval, P. Porion, H. Van Damme, J. Phys. Chem. B 103 (1999) 5730–5735.
[23] E. Cloutis, Analytical data for mineral and rock samples, HOSERLab Mineral Database, University of Winnipeg (accessed on 09.06.14), http://psf.uwinnipeg.ca/Sample_Database_files/Mineral_database_latest.doc.
[24] R. Cotts, M. Hoch, T. Sun, J. Markert, J. Magn. Reson. 1989 (83) (1969) 252–266.
[25] P.T. Callaghan, Principles of Nuclear Magnetic Resonance Microscopy, Oxford University Press, 1993.
[26] M. Holtz, S. Heil, A. Sacco, Phys. Chem. Chem. Phys. 2 (2000) 4740–4742.
[27] H. Weingärtner, Ber. Bunsenges. Phys. Chem. 88 (1984) 47–50.
[28] J. Crank, The Mathematics of Diffusion, Oxford University Press, 1979.
[29] D. van der Beek, H. Reich, P. van der Schoot, M. Dijkstra, T. Schilling, R. Vink, M. Schmidt, R. van Roij, H. Lekkerkerker, Phys. Rev. Lett. 97 (2006) 087801.
[30] I.C. Bourg, G. Sposito, J. Colloid Interface Sci. 360 (2011) 701–715.
[31] C.T. Johnston, Clay Miner. 45 (2010) 245–279.
[32] Y. Nakashima, F. Mitsumori, Appl. Clay Sci. 28 (2005) 209–221.
[33] S. Abend, G. Lagaly, Appl. Clay Sci. 16 (2000) 201–227.
[34] S. Karaborni, B. Smit, W. Heidug, J. Urai, E. Van Oort, Science 271 (1996) 1102–1104.